analytical chemistry

Article

Cite This: Anal. Chem. 2019, 91, 1269−1276

pubs.acs.org/ac

Sum Frequency Generation Imaging Microscopy of Self-Assembled Monolayers on Metal Surfaces: Factor Analysis of Mixed Monolayers

Aleksandr A. Pikalov, Dien Ngo, Han Ju Lee, T. Randall Lee, and Steven Baldelli*

Department of Chemistry, University of Houston, Houston, Texas 77204-5003, United States

Supporting Information

ABSTRACT: Sum frequency generation (SFG) images of microcontact patterned self-assembled alkanethiol monolayers on metal surfaces were analyzed by factor analysis (FA) to determine the spatial distribution of the patterned monolayers over the images. Additionally, each significant abstract factor produced by FA was assessed to determine the information contained within it. These results indicate that FA of the SFG spectra is a promising method to determine the composition and identities of mixed alkanethiol systems that show different vibrational spectra and image contrast. Factor analysis has successfully been applied to SFG images obtained with low signals, which reduces the time required for full spectral SFG imaging.

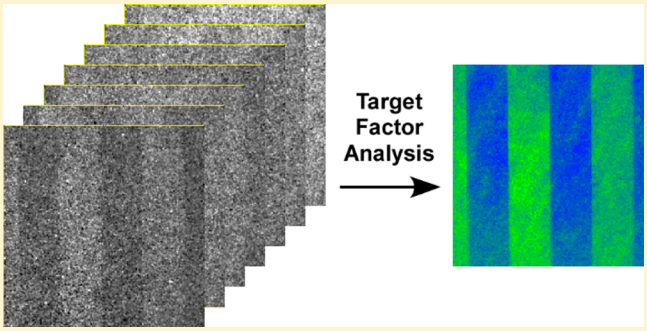

Surfaces and interfaces are considered as a boundary between a material and its surrounding environment and influence interactions with that environment. At the molecular level, the surface atoms, the top 1−10 atomic layers, have a different chemical and physical environment than an atom in the bulk and play an important role in many of the chemical, physical, and biological processes.[1,2] In order to gain a fundamental understanding of the underlying processes, it is critically important to know the chemical and physical properties of the surfaces or interfaces. To investigate surface properties, model systems like self-assembled monolayers (SAMs) have been used.[3,4] A self-assembled monolayer is an organized layer of organic molecules adsorbed on a substrate surface. These SAMs are easy to prepare, are molecularly ordered, and are robust under many conditions of use. In order to control the surface chemically and spatially, patterned systems of mixed SAMs have been utilized. These patterned SAMs systems have been produced by many different techniques like microcontact printing,[5−7] photolithography,[8] lift-off-lithography,[9] and inkjet printing.[10] Microcontact printing (μCP) is a form of soft lithography method that uses a polydimethylsiloxane (PDMS) stamp to form patterns of SAMs on the metal surface in a patterned and controlled fashion.[5−7] The advantage of using PDMS is that it absorbs SAMs onto its surface and releases them during stamping. It is also nontoxic, commercially available, compatible with wide variety of organic and organometallic molecules, and unreactive toward most chemicals.[5]

Self-assembled monolayer patterned surfaces have been characterized by techniques such as X-ray photoelectron spectroscopy (XPS), secondary ion mass spectrometry (SIMS), low energy electron diffraction (LEED), and scanning probe microscopy techniques (STM, AFM), but each technique has advantages and disadvantages.[11−15] These techniques show the structures of the monolayers but require other techniques, such as vibrational spectroscopy, to determine the molecular composition of the surface.[16] Sum frequency generation (SFG) spectroscopy is a second-order, nonlinear optical technique that provides vibrational spectra of the molecules at the interface.[17] Chemical identification, molecular orientation, monolayers' conformational order, and vibrational dynamics can be studied by SFG spectroscopy.[18,19] The technique is very useful in providing information about the interfacial structure of a surface. However, it typically only provides the average information on the sampled area and does not show local characteristics due to the spatial averaging. The sum frequency generation imaging microscopy (SFG-IM) technique, based on SFG, provides chemical images of the surface.[20−23] The chemical contrast is based on the vibrational frequencies of the adsorbed molecules on the surface. The advantage of using SFG-IM to study patterned surfaces is that it not only provides the identity of surface/interface molecular species, information about surface/interface chemical structure, but it also provides a spatial distribution overview of chemicals on the surface, which make it a useful technique in chemical imaging.[21,24]

In this study, SFG-IM was used to acquire SFG images of patterned alkanethiol monolayer on gold by μCP. The images were then analyzed by factor analysis (FA). It is a statistical method that uses mathematical procedures to investigate whether a number of observed variables are linearly related to

Received: April 24, 2018
Accepted: December 17, 2018
Published: January 3, 2019

DOI: 10.1021/acs.analchem.8b01840
Anal. Chem. 2019, 91, 1269−1276

some smaller number of unobservable factors.[25] The method has been applied in Raman and infrared spectroscopy to determine the number and identities of components in a series of related multicomponent mixtures.[26−30] The focus of these experiments was to investigate the application of FA on SFG images and to assess the chemical maps and abstract factors produced by FA.

THEORETICAL BACKGROUND

Sum Frequency Generation. The theory of SFG has been described previously in detail.[16,18] The sum frequency generation process in this study is achieved when two coherent laser pulses, a fixed wavelength of 1064 nm ($\omega_{1064\ nm}$) and a tunable wavelength infrared pulse (ω_{IR}), are spatially and temporally overlapped on a surface. The induced nonlinear polarization at the surface generates the coherent sum frequency output beam at the sum of the two input beam frequencies ($\omega_{SF} = \omega_{1064\ nm} + \omega_{IR}$). When the IR frequency is at a resonance frequency of one of the vibrational modes, an enhanced SFG signal is observed.

Factor Analysis. The theory and application of factor analysis (FA) are discussed fully by Malinowski.[31] A short description of the main steps are given in the Supporting Information. Factor analysis is a mathematical technique for studying matrices of data. It is a highly useful method for furnishing the number of components, concentrations, and spectral information via a purely mathematical route.[31] It is performed by taking a data set of interest D and, after decomposition, expressing it as a linear sum of product terms. The resulting terms are purely mathematical "abstract" column and row factors that contain no physical or chemical meaning. To acquire physically or chemically recognizable factors, a transformation of the abstract factors is required. Target testing is a unique transformation method that tests potential factors, known as target factor analysis (TFA).[31] Target testing serves as a mathematical bridge between abstract and real factors. Factor analysis includes principle component analysis (also known as principal factor analysis (PFA)) and TFA,[31] and their use for this study is outlined in the Experimental Section.

EXPERIMENTAL SECTION

Sample Patterning by Microcontact Printing. The system of study consisted of patterned SAMs on gold substrate manufactured by microcontact printing (μCP). The PDMS stamp used for μCP was produced by combining the PDMS prepolymer and curing agent in a 10:1 volume ratio. After stirring for about 5 min, the mixture was placed under house vacuum for about an hour to remove bubbles produced during mixing. It was then poured onto a clean surface of the rigid master pattern, previously treated with octadecyltrichlorosilane as an antiadhesion layer for easy peeling of PDMS from the master pattern. Then, the master pattern with the PDMS mixture was placed inside the oven to cure for 2 h at 80 °C. After curing, the PDMS was carefully peeled off from the master pattern and cleaned by sonicating in ethanol.

Pure solutions of 5 mM octadecanethiol (ODT), methoxy-hexadecanethiol (MeOHT), and 15,15-difluoro-octadecane-1-thiol (FODT) in ethanol were prepared. To prepare the two-component monolayer samples, a drop of the ODT solution was placed on top of the PDMS stamp and then nitrogen gas was used to dry the surface of the stamp. The stamp was then carefully placed on the surface of evaporated gold on silicon wafer for 15 min. After the stamp was removed, the sample was placed into the backfill solution (MeOHT or FODT) for 15 min. Target samples for TFA application were prepared from the same solutions as the two component samples. The stamped ODT target sample was prepared by the same procedure described above but without backfilling. MeOHT and FODT target samples were prepared by solution deposition, with no stamping, for 15 min of the respective MeOHT or FODT solution on evaporated gold silicon wafer. All samples were rinsed with ethanol solvent and dried with nitrogen gas before taking images.

Sum Frequency Generation Imaging Microscope. A picosecond pulsed, 20 Hz, Nd:YAG laser was used to generate the 1064 nm, which pumped the optical parametric generator/amplifier (OPG/OPA) to generate the tunable mid-IR beam. The incident angles of the 1064 nm and mid-IR beams were set to 60° and 70° from the surface normal, respectively, and generated the SFG beam at around 800 nm with an angle of approximately 62.1° from the surface normal. An intensified charge-coupled device (iCCD) camera with a 1024 × 1024 pixel chip was used to acquire the SFG images. A more detailed description of the SFG-IM is given in the Supporting Information.

SFG Image Data Processing with PFA and TFA Application. During the SFG imaging, the iCCD camera acquires a sequence of SFG images, while the infrared frequency is continuously scanned at a set scan rate. Each image is an average of five IR wavenumbers, with a user specified number of laser shots per image. No processing of the presented SFG images were performed except for background correction. Once a set of images was acquired, the images were stacked according to decreasing IR wavenumber using ImageJ software. The image stack was cut into region of interests (ROIs) of 5-by-5 and 2-by-2 pixels, which corresponds to 6.5-by-6.5 μm and 2.5-by-2.5 μm respectively, and vibrational spectra were extracted from each ROI (see Figure S-1).[32] The extracted spectra from ROIs were then used to construct a matrix, where each spectrum is a column of the data matrix, on which the PFA and TFA were performed using MATLAB software. The MATLAB codes for PFA and TFA are provided by Malinowski.[31]

The data matrices were first analyzed by PFA to determine the number of significant factors using factor (empirical) indicator function (IND).[31] The IND function reaches a minimum when the correct number of factors were employed and are considered significant. A more detailed explanation is given in the Supporting Information. To obtain abstract factors, the data matrices were decomposed using the singular value decomposition (SVD) function in MATLAB. The significant abstract factors from the C (column) matrices were used to construct maps of each abstract factors' contributional weight in each ROI; R (row) matrices abstract factors were used to produce the corresponding abstract factors' spectra. No further processing was performed on the abstract factors' spectra and maps presented. When it is possible, test (target) spectra of pure components were used to produce the transformation matrix to convert abstract factors into physically significant real factors. The resulting real factors were used to construct the respective chemical maps. The chemical maps were constrained to positive values only with no other constraints or processing.

DOI: 10.1021/acs.analchem.8b01840
Anal. Chem. 2019, 91, 1269−1276

RESULTS AND DISCUSSION

SFG Imaging of ODT-MeOHT Sample. The SFG images and spectra given in Figure 1 represent the ODT-MeOHT on

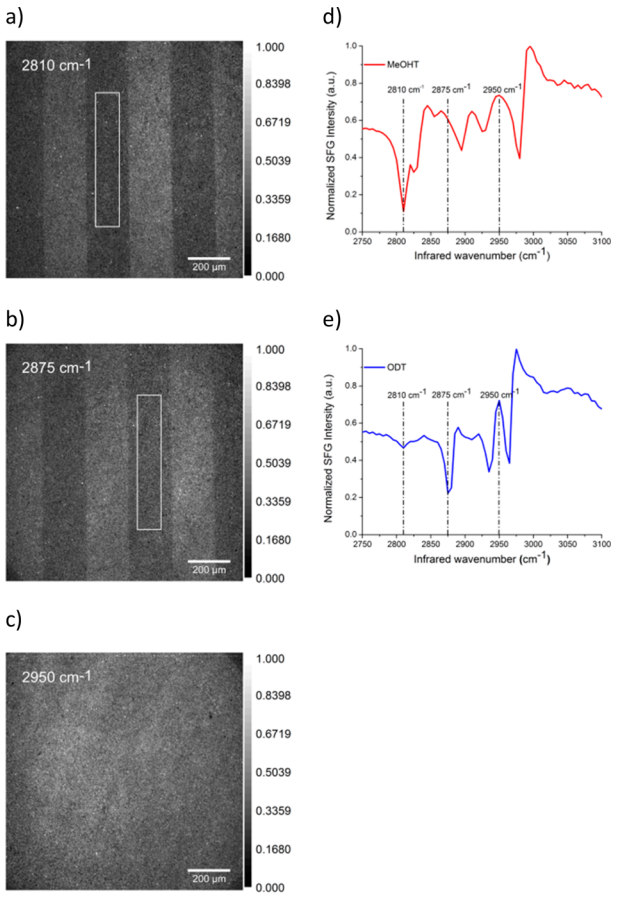

Figure 1. ODT-MeOHT sample SFG images at (a) 2810 cm^{-1}, (b) 2875 cm^{-1}, (c) 2950 cm^{-1}, (d) MeOHT SFG spectrum, and (e) SFG spectrum of ODT stamped region.

an evaporated gold substrate sample. Figure 1a–c shows SFG images taken at 2810, 2875, and 2950 cm^{-1}, respectively. The spectra shown in Figure 1d and e were extracted from the ROI highlighted in Figure 1a and b, respectively. The observed SFG image contrast is due to the vibrational contrast in the SFG spectra, where the dark areas in the images correlate to the resonance peaks in the SAMs. ODT and MeOHT have distinct vibrational spectra in the 2800–3000 cm^{-1} region that can be used to distinguish the two molecules. Figure 1d and e are the characteristic SFG MeOHT and ODT spectra, respectively, on gold. The MeOHT shows six peaks in the C–H stretching region, a doublet at 2810/2830, 2855, 2900, 2930, and 2980 cm^{-1}, which correspond to the symmetric stretch of the CH_3 in the terminal methoxy group, CH_2 symmetric stretch, CH_2 asymmetric stretch, Fermi resonance, and the CH_3 antisymmetric stretch, respectively. The peaks in Figure 1e at 2875 and 2935 cm^{-1} are the methyl symmetric C–H stretch and its Fermi resonance, respectively, and at 2965 and 2975 cm^{-1} are the methyl antisymmetric in-plane and out of plane stretching, respectively. The observed methoxy peak at 2810 cm^{-1} in the ODT spectrum is due to the MeOHT mixing in the ODT stamped region during the backfill step which is most likely due to stamp defects and also that the overall monolayer formed by microcontact printing is less densely packed than those from solution-deposited films.[22] The observed dark areas of the SFG image at 2810 cm^{-1} correspond to the MeOHT covered surface, which has a symmetric methoxy stretch at that frequency, and lighter areas correspond to the ODT surface, which has no vibrational modes at that frequency and signal is due to Au nonresonant response. The image contrast inverts at 2875 cm^{-1} due to MeOHT being off resonance while the methyl-terminated ODT is at resonance. When both the MeOHT and ODT are off vibrational resonant frequencies, little image contrast is observed. An example of an off vibrational resonant image is shown in Figure 1c.

Two Component Maps. Chemical maps have been constructed from SFG images using spectral fitting which requires sufficient signal-to-noise ratio of the individual spectra. This limits the spectral curve-fitting to larger ROIs or long signal acquisition times.[32−34] In order to reduce signal acquisition time without resorting to larger ROIs or sacrificing image resolution, factor analysis was utilized. SFG images of ODT-MeOHT sample were acquired at 5000 shots per image (5k) and also at 500 shots per image (0.5k). The SFG images were processed as outlined in the SFG imaging data processing with PFA and TFA application. The SFG and resulting PFA images are shown in Figure 2. Figure 2a and b are the raw SFG

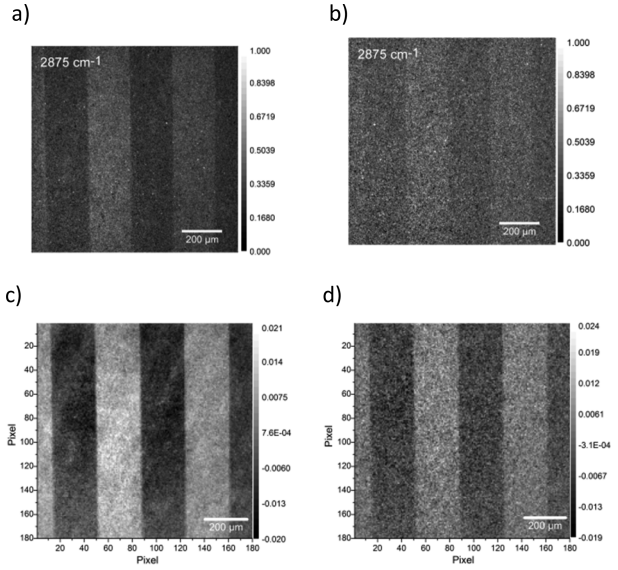

Figure 2. ODT-MeOHT sample SFG images acquired with (a) 5k shots per image at 2875 cm^{-1} and (b) 0.5k shots per image at 2875 cm^{-1}. PFA resulting maps of 6.5-by-6.5 μm ROI (c) 5k shots per image 2nd abstract factor and (d) 0.5k shots per image 3rd abstract factor.

images acquired at 2875 cm^{-1} with 5k and 0.5k, respectively. The contrast between the ODT and MeOHT regions in Figure 2b is not as high as in Figure 2a and is difficult to determine where the regions boundary edge is due to low edge resolution. However, the images obtained after PFA processing of the 5k and 0.5k, Figure 2c and d, respectively, show an improved region contrast and edge resolution. As observed in Figure 2b,d, PFA significantly improves the image contrast between the ODT and MeOHT regions for the 0.5k data compared to the 5k data. The extracted SFG spectra of ODT and MeODT of the 0.5k sample using 6.5-by-6.5 μm ROI size for PFA do not contain sufficient signal to show obvious vibrational modes that could be used to differentiate ODT from MeOHT (see

DOI: 10.1021/acs.analchem.8b01840
Anal. Chem. 2019, 91, 1269–1276

Figure S-2) required for spectral fitting. To understand and be able to determine the significance of PFA and TFA results, the 5k SFG data was analyzed to determine what each significant real and abstract factor represented. Then, 0.5k real and abstract factors were compared to the 5k factors to determine if the real and abstract factors represented the same information in the 0.5k as the 5k data set. To test the limit of PFA, 100 shots per image SFG data was analyzed with PFA but due to the low SFG signal, PFA was unable to determine the number of significant factors nor produce satisfactory results (see Figures S-3 and S-4).

Analysis of 5000 Laser Shots Per Image ODT-MeOHT Sample. Principal factor analysis produced 71 abstract factors, due to each spectrum used for the data matrix consisting of 71 data points, but IND function indicated only two significant abstract factors that account for 91.7% of data variance. The 69 nonsignificant abstract factors account for 8.3% of data variance and are assumed to contain only noise. The percent contribution of each abstract factor was calculated from eigenvalues. After target transformation by TFA of the abstract factors using ODT and MeOHT target spectra, the resulting component weights of ODT and MeOHT were obtained in each ROI. The component weight results were then mapped back onto the surface to provide a spatial distribution of the MeOHT and ODT shown in Figure 3a–d. Figure 3a and b are

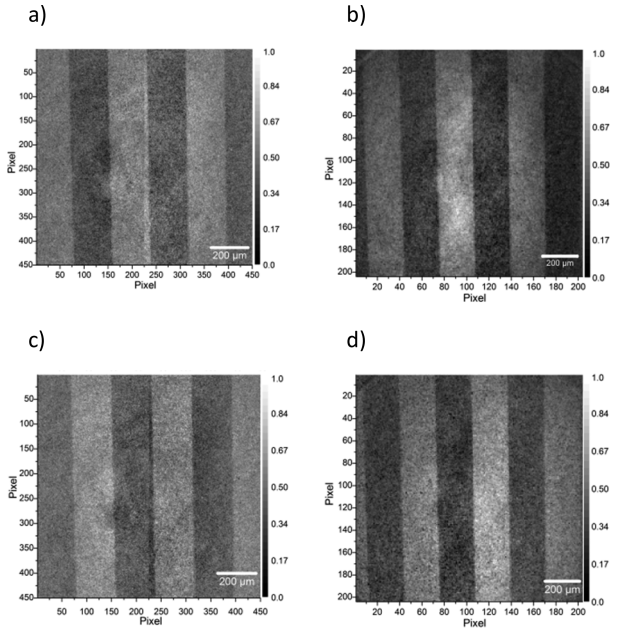

Figure 3. MeOHT and ODT chemical maps. (a) MeOHT using 2.5-by-2.5 μm ROIs, (b) MeOHT from 6.5-by-6.5 μm ROIs, (c) ODT using the 2.5-by-2.5 μm ROIs, and (d) ODT from 6.5-by-6.5 μm ROIs. Note: data matrix containing the 2.5-by-2.5 μm ROIs was too large for the computer calculations as a whole. It was divided into six equal fractions, and TFA calculations were performed on each individually. The TFA results were then combined to produce the final images shown in a and c.

the MeOHT chemical maps constructed from 2.5-by-2.5 μm and 6.5-by-6.5 μm ROIs, respectively, where the MeOHT regions are represented by lighter shaded region. Figure 3c and d are the ODT chemical maps constructed from 2.5-by-2.5 μm and 6.5-by-6.5 μm ROIs, respectively, where the ODT regions are represented by lighter regions. The chemical maps of MeOHT and ODT obtained by TFA are in good agreement with the observed SFG image in Figure 1b. The TFA results of ODT and MeOHT images shown in Figure 3 are the physically significant real factors obtained by target transformation of the abstract factors. The mathematical process by which the significant abstract factors are target transformed to produce the real factors is graphically shown in Figure S-5. The MeOHT and ODT were obtained by taking weighted fractions of the two significant factors and subtracting the second abstract factor from the first one to obtain MeOHT image or adding them together to obtain ODT image.

The two significant abstract factors obtained by PFA as are shown in Figure 4. First abstract factor accounts for 91% of the

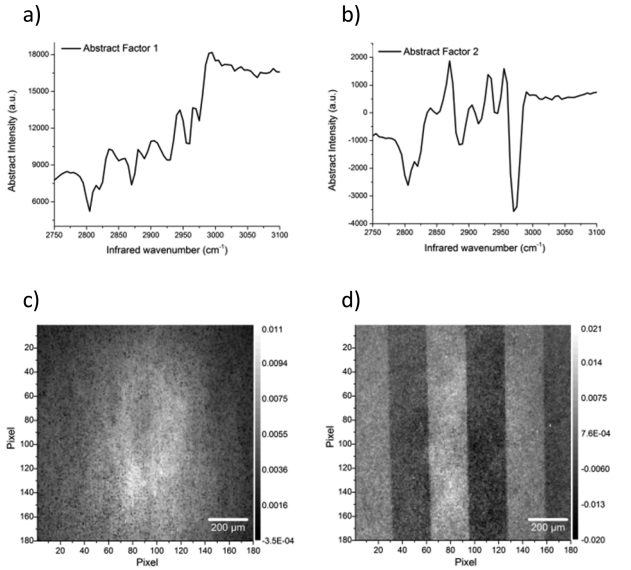

Figure 4. First and second abstract factors from row matrix (a, b) and column matrix (c, d) obtained by PFA of ODT-MeOHT sample data matrix.

data matrix variance and since the spectra was not mean centered, it represents the average spectrum of the sample analyzed.[35] Figure 4a and c show the first abstract factor extracted from the R and the corresponding C matrix, respectively. In Figure 4a, the observed mathematical results are the combined average of the ODT and MeOHT SFG signal response on gold substrate, where all the ODT and MeOHT vibrational peaks observed in Figure 1d,e are present. Figure 4c represents an overall beam profile over the imaged area, with no image contrast between the ODT and MeOHT regions. The second abstract factor accounts for 0.74% of data variance. The R matrix component of the second factor is shown in Figure 4b and represents the spectral difference between the observed ODT and MeOHT peak positions.[35] It also contains both the ODT and MeOHT spectral features, but in derivative-like shapes where the ODT peaks are pointing up and MeOHT peaks are pointing down. In Figure 5, the abstract factor is overlaid with the SFG difference spectrum of ODT and MeOHT, showing that the second abstract factor represents the difference spectra of ODT and MeOHT. The SFG difference spectrum of ODT and MeOHT was acquired by subtracting normalized ODT spectrum from normalized MeOHT spectrum (see Figure S-6).[36] It has been observed that one vibrational band disappearing relative to another in the spectrum will produce a factor containing one negative and

DOI: 10.1021/acs.analchem.8b01840
Anal. Chem. 2019, 91, 1269–1276

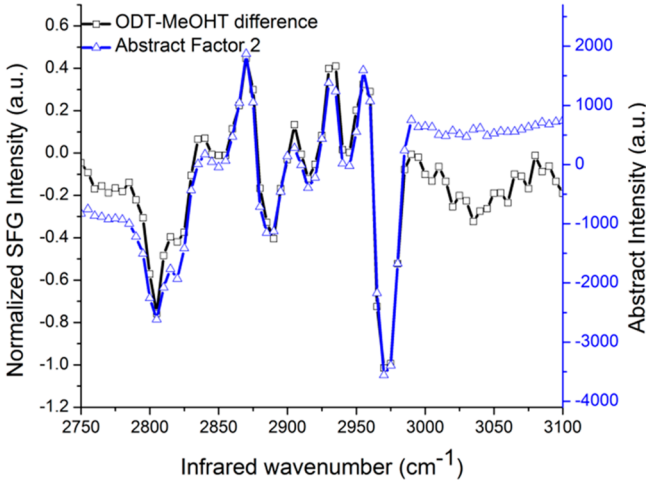

Figure 5. Resulting SFG spectrum of ODT and MeOHT after normalized ODT SFG spectrum was subtracted from the normalized MeOHT SFG spectrum and compared with the second abstract factor obtained from PFA.

one positive weighted peak.[35] The corresponding second factor from the *C* matrix, Figure 4d, contains the image contrast between the ODT and MeOHT regions. Darker strips are the ODT regions and lighter stripes are the MeOHT regions. The contrast is maximized between the two regions by expressing one as positive values and the other one as negative values.[35] The PFA results shown in Figure 4 are considered abstract mathematical results that contain no physically meaningful information, but based on Figures 4 and 5, they do contain real physical information.[35] In order to determine the significance of the information contained in the abstract factors, one must have some insight into the system analyzed. By analyzing the abstract factor one can narrow down the potential targets to test.

Analysis of ODT-MeOHT Sample Obtained with 500 Laser Shots per Image. SFG images acquired of ODT-MeOHT sample with 500 laser shots per image are shown in Figure 6. The contrast between the ODT and MeOHT regions in Figure 6a,b is not as high as in Figure 1a,b, which were taken with 5000 shots per image. The 0.5k ODT-MeOHT stack was treated in the same manner as the 5k ODT-MeOHT stack. The IND function indicated three significant abstract factors, not two, as was expected and observed for the 5k data. The first three abstract factors obtained by PFA are shown in Figure 7 and account for 81.2% of data variance. The first abstract factor shown in Figure 7a,d contains 79.2% of data variance and is almost identical to the first factor of 5k (Figure 4a,c). It also represents the combined average spectrum of the ODT and MeOHT spectra and the beam profile of the imaged area, containing both the ODT and MeOHT peaks but showing no image contrast between the two regions. The second abstract factor, shown in Figure 7b,e, represents 1.3% of data variance and is different than the second abstract factor of 5k sample (Figure 4b,d). It is assumed to represent some change to the combined average spectrum that has not been fully determined yet or might be a result of increased noise in the data. The third abstract factor accounts for 0.72% of the input data matrix. The *R* matrix component, Figure 7c, is very similar to the second abstract factor of the 5k (Figure 4b), which represents a difference like spectrum of ODT and MeOHT, where SFG spectrum of ODT was subtracted from MeOHT

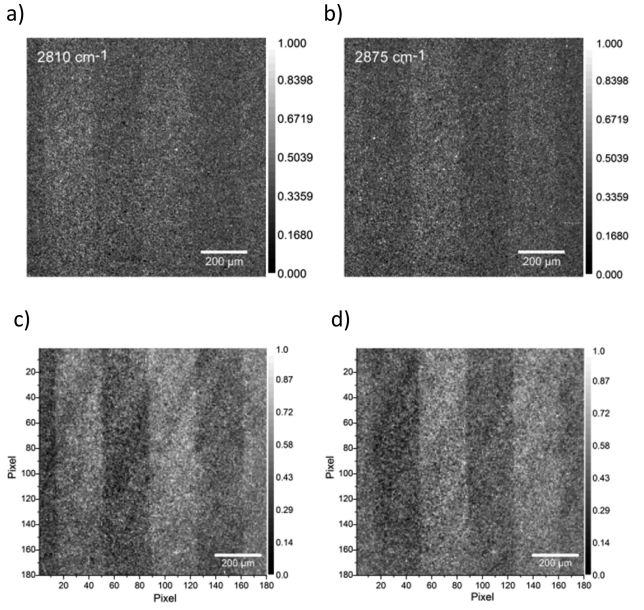

Figure 6. 500 shot ODT-MeOHT sample SFG images at (a) 2810 cm^{-1} and (b) 2875 cm^{-1}, and TFA resulting maps of 6.5-by-6.5 μm ROI (c) MeOHT and (d) ODT.

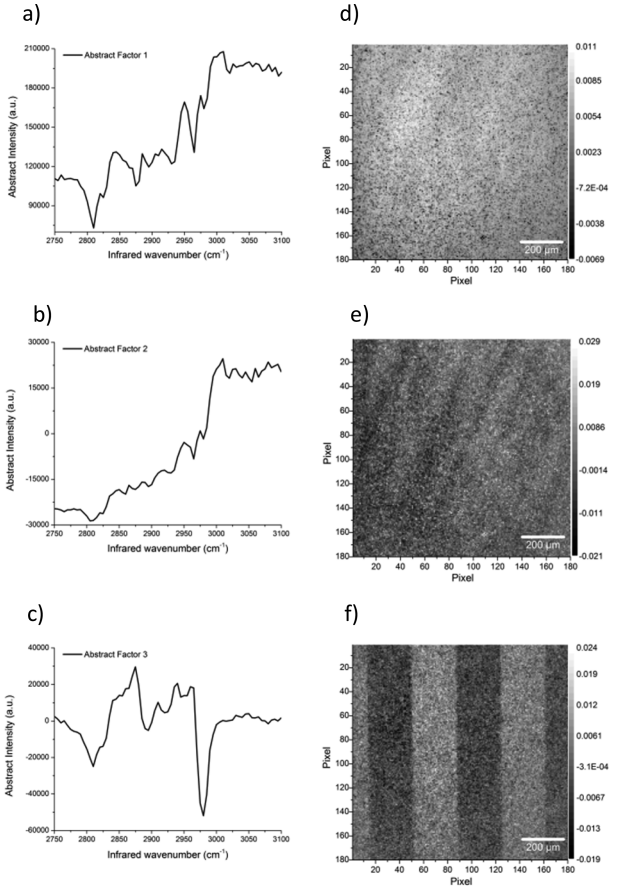

Figure 7. First three abstract factors from row matrix (a−c) and column matrix (d−f) obtained by PFA of 500 shot ODT-MeOHT sample data matrix.

spectrum. The contrast between ODT and MeOHT regions observed in Figure 7f is maximized by expressing one as positive values and the other one as negative values, which is

DOI: 10.1021/acs.analchem.8b01840
Anal. Chem. 2019, 91, 1269−1276

similar to what was previously observed for the second abstract factor of 5k (Figure 4d). The abstract image obtained from the 0.5k data set (Figure 7f) is not as detailed and lacks the resolution, especially between the boundary of ODT and MeOHT regions, when compared to the image obtained from the 5k data set (Figure 4d). These results demonstrate that PFA can provide very similar qualitative chemical image results from data obtained with 1/10th the shots per spectral point as originally obtained. This also demonstrates that FA can be used as an alternative chemical mapping to spectral fitting. The FA and TFA results of smaller ROIs and shorter acquisition time data indicate that FA can reduce the amount of time required to acquire full spectral images with sufficient contrast between the different chemical regions when compared to spectral fitting.

Analysis of ODT-Fluoro-ODT Sample. The ODT and FODT molecules exhibit almost identical spectra except that the $-CH_3$ symmetric and asymmetric stretches differ (relative shifted blue for FODT) by 5 cm^{-1} (Figure 8b). The structural

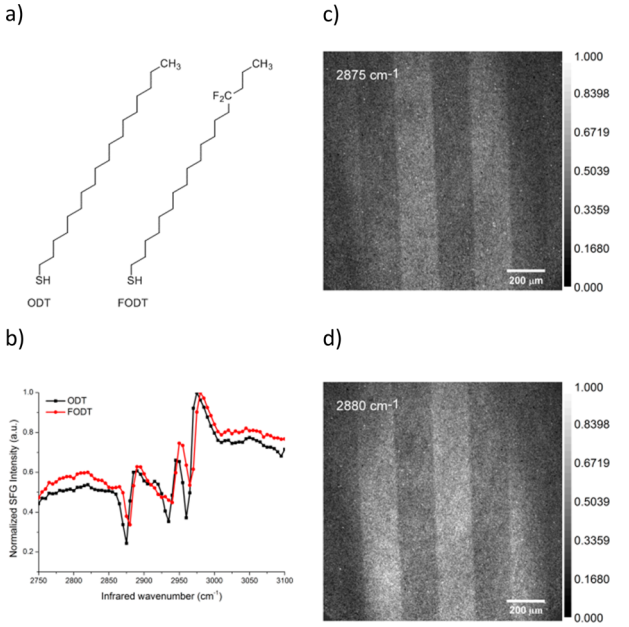

Figure 8. (a) ODT and FODT molecular structure. ODT-FODT sample SFG (b) spectra and (c) image at 2875 cm^{-1} and (d) 2880 cm^{-1} with 5000 shots.

difference between the ODT and FODT molecules is that FODT contains two fluorines at the 15th carbon position (Figure 8a). SFG imaging was taken of ODT-FODT sample with 5000 laser shots per image. The SFG images taken at 2875 and 2880 cm^{-1}, Figure 8c and d, respectively, show good contrast between the ODT stamped region and fluorinated thiol backfilled region represented by darker shaded regions in the respective images. The stack of ODT-FODT SFG images were treated the same as the ODT-MeOHT SFG images.

Principal factor analysis results indicated that there are three significant abstract factors that account for 96.5% of data variance. The 3.5% account for the 68 nonsignificant abstract factor that are assumed to contain only noise. Target testing of ODT and FODT by TFA revealed that both ODT and FODT are real factors of the data analyzed. The three significant abstract factors produced by PFA are shown in Figure 9. The first abstract factor accounts for 95.7% of input data matrix.

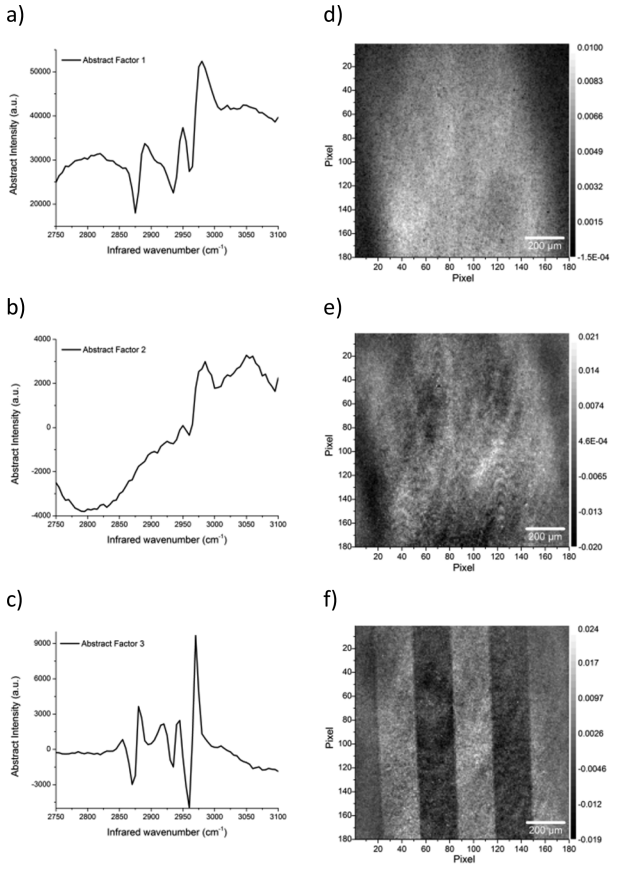

Figure 9. First three abstract factors from row matrix (a–c) and column matrix (d–f) obtained by PFA of ODT-FODT sample data matrix.

The *R* matrix component of the factor, Figure 9a, represents the average spectrum of the data matrix and is almost identical to the SFG spectra of ODT (Figure 10a), which might be due to ODT and FODT spectra being almost identical, except for the methyl symmetric and asymmetric stretches that are shifted by 5 cm^{-1}. The SFG spectral resolution is 5 cm^{-1}, where only a shift by one data point will result in the first abstract factor to resemble either ODT or FODT. The corresponding first abstract factor of *C* matrix, Figure 9d, represents the SFG beam intensity signal over the image area. The second abstract factor, Figure 9b,e, accounts for 0.51% of the input data matrix and represent some change to the first abstract factor that has not been determined yet, but has been observed in the 0.5k MeOHT-ODT results (Figure 7b,e). The third factor accounts for 0.28% of the input data matrix. The *R* matrix component, Figure 9c, represents the spectral difference between the observed ODT and FODT peak positions in derivative-like shapes.[35] It contains both the ODT and FODT spectral information where the ODT peaks are pointing down and FODT peaks are pointing up. When compared to the SFG ODT and FODT spectra, it represents the difference spectrum of ODT and FODT (Figure 10b), where SFG spectrum of FODT was subtracted from ODT spectrum which is similar to what was previously observed for the second abstract factor of ODT-MeOHT sample. The corresponding *C* matrix component, Figure 9f, contains the image contrast between the ODT and FODT regions, where the darker and lighter regions of the image represent ODT and FODT regions respectively, which

DOI: 10.1021/acs.analchem.8b01840
Anal. Chem. 2019, 91, 1269–1276

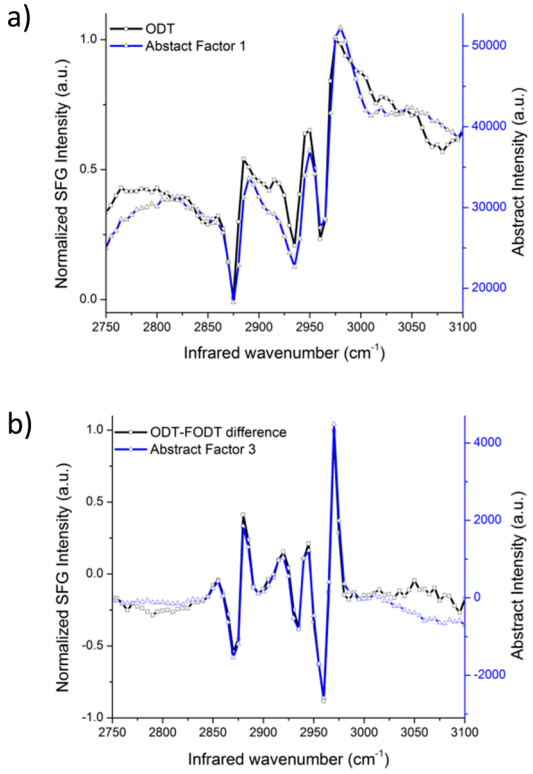

Figure 10. (a) First abstract factor compared with SFG spectrum of ODT, and (b) resulting SFG spectrum of ODT and FODT after normalized FODT SFG spectrum was subtracted from the normalized ODT SFG spectrum compared with the third abstract factor obtained from PFA.

is in good agreement with SFG image of ODT and FODT shown in Figure 8c.

CONCLUSION

This work has shown that PFA and TFA can be used successfully on low signal data to extract individual species spectral information, and also the spatial distribution of chemically different alkanethiols on gold surface. In this study, the chemical systems studied have consisted of two components, where the chemical species used here have distinctly different vibrational spectra, in the case of ODT and MeOHT, and very similar vibrational spectra, in the case of ODT and FODT. The resulting chemical maps have demonstrated that TFA can be successfully applied to SFG images to acquire real significant factors. It also shows that PFA can be applied just as successfully to data obtained with lower signal or with shorter acquisition times. The reconstructed chemical maps indicate that TFA can be utilized as an alternative to spectral fitting to generate chemical maps. This work has demonstrated that caution should be exercised when determining the number of chemical components present and which factors represent the corresponding components. The decomposition step produces abstract factors that do not necessary represent the chemical components individually but may represent some other inherent underlying principles responsible for producing the data results analyzed. It has been observed that the number of significant factors do not always correspond to the number of components present. The components are not necessarily represented by the first or even the second abstract factor and may be represented by one factor or multiple factors or a combination of factors. It is considered that factors or components obtained by PFA are just mathematical results that contain no physical or chemical meaning but as this work has shown that they might contain meaningful information. It is important to remember that it is difficult to determine what factors contain the chemical species spectral information without targets. More studies need to be conducted to determine the effectiveness of FA on real samples that contain mixed unknown chemical species and random patterns.

ASSOCIATED CONTENT

Supporting Information

The Supporting Information is available free of charge on the ACS Publications website at DOI: 10.1021/acs.analchem.8b01840.

Sum frequency generation imaging microscope, factor analysis, illustration of imaging stacking and spectral extraction, 100 shots per image SFG image and FA results, and an outline of target transformation of abstract factor into real factors (PDF).

AUTHOR INFORMATION

Corresponding Author

*E-mail: sbaldelli@uh.edu.

ORCID

Dien Ngo: 0000-0001-9415-2731
T. Randall Lee: 0000-0001-9584-8861
Steven Baldelli: 0000-0002-5747-259X

Notes

The authors declare no competing financial interest.

ACKNOWLEDGMENTS

We would like to thank Daniela Rodriguez for providing MeOHT. We gratefully acknowledge the NSF (CHE-1361885) for providing funds for this project. T.R.L. wishes to thank the NSF (CHE-1710561), the Robert A. Welch Foundation (E-1320), and the Texas Center for Superconductivity at the University of Houston for providing generous support for this research.

REFERENCES

(1) Somorjai, G. A.; Li, Y. *Introduction to Surface Chemistry and Catalysis*, 2nd ed.; Wiley: Hoboken, N.J., 2010; p xii.
(2) Somorjai, G. A.; Li, Y. M. *Proc. Natl. Acad. Sci. U. S. A.* **2011**, *108*, 917−924.
(3) Bain, C. D.; Whitesides, G. M. *Angew. Chem., Int. Ed. Engl.* **1989**, *28*, 506−512.
(4) Schreiber, F. *J. Phys.: Condens. Matter* **2004**, *16*, R881−R900.
(5) Kumar, A.; Biebuyck, H. A.; Whitesides, G. M. *Langmuir* **1994**, *10*, 1498−1511.
(6) Ruiz, S. A.; Chen, C. S. *Soft Matter* **2007**, *3*, 168−177.
(7) Thakar, R.; Baker, L. A. *Anal. Methods* **2010**, *2*, 1180−1183.
(8) Shadnam, M. R.; Kirkwood, S. E.; Fedosejevs, R.; Amirfazli, A. *Langmuir* **2004**, *20*, 2667−2676.
(9) Liao, W. S.; Cheunkar, S.; Cao, H. H.; Bednar, H. R.; Weiss, P. S.; Andrews, A. M. *Science* **2012**, *337*, 1517−1521.
(10) Pardo, L.; Wilson, W. C.; Boland, T. J. *Langmuir* **2003**, *19*, 1462−1466.
(11) Vericat, C.; Vela, M. E.; Benitez, G. A.; Gago, J. A. M.; Torrelles, X.; Salvarezza, R. C. *J. Phys.: Condens. Matter* **2006**, *18*, R867−R900.

DOI: 10.1021/acs.analchem.8b01840
Anal. Chem. 2019, 91, 1269−1276

(12) Grunthaner, F. J.; Grunthaner, P. J.; Vasquez, R. P.; Lewis, B. F.; Maserjian, J.; Madhukar, A. *Phys. Rev. Lett.* **1979**, *43*, 1683−1686.
(13) Toselli, M.; Gardella, J. A.; Messori, M.; Hawkridge, A. M.; Pilati, F.; Tonelli, C. *Polym. Int.* **2003**, *52*, 1262−1274.
(14) Vickerman, J. C.; Gilmore, I. *Surface Analysis: The Principal Techniques*, 2nd ed.; John Wiley & Sons: Chichester, U.K., 2009; p *xix*.
(15) Woodruff, D. P.; Delchar, T. A. *Modern Techniques of Surface Science*, 2nd ed.; Cambridge University Press: New York, 1994; p *xviii*.
(16) Bain, C. D. *J. Chem. Soc., Faraday Trans.* **1995**, *91*, 1281−1296.
(17) Zhu, X. D.; Suhr, H.; Shen, Y. R. *Phys. Rev. B: Condens. Matter Mater. Phys.* **1987**, *35*, 3047−3050.
(18) Wang, H. F.; Gan, W.; Lu, R.; Rao, Y.; Wu, B. H. *Int. Rev. Phys. Chem.* **2005**, *24*, 191−256.
(19) Wang, H. F. *Prog. Surf. Sci.* **2016**, *91*, 155−182.
(20) Florsheimer, M.; Brillert, C.; Fuchs, H. *Mater. Sci. Eng., C* **1999**, *8*−*9*, 335−341.
(21) Hoffmann, D. M. P.; Kuhnke, K.; Kern, K. *Proc. SPIE* **2002**, *4812*, 82−90.
(22) Cimatu, K.; Baldelli, S. *J. Phys. Chem. B* **2006**, *110*, 1807−1813.
(23) Cimatu, K.; Baldelli, S. *J. Am. Chem. Soc.* **2006**, *128*, 16016−16017.
(24) Fang, M.; Baldelli, S. *J. Phys. Chem. C* **2017**, *121*, 1591−1601.
(25) Rostami, A.; Abdollahi, H.; Maeder, M. *Anal. Chim. Acta* **2016**, *911*, 35−41.
(26) Mccue, M.; Malinowski, E. R. *Anal. Chim. Acta* **1981**, *133*, 125−136.
(27) Ngo, D.; Baldelli, S. *J. Phys. Chem. B* **2016**, *120*, 12346−12357.
(28) Woods, D. A.; Petkov, J.; Bain, C. D. *Colloids Surf., A* **2011**, *391*, 10−18.
(29) Woods, D. A.; Petkov, J.; Bain, C. D. *J. Phys. Chem. B* **2011**, *115*, 7353−7363.
(30) Woods, D. A.; Petkov, J.; Bain, C. D. *J. Phys. Chem. B* **2011**, *115*, 7341−7352.
(31) Malinowski, E. R. *Factor Analysis in Chemistry*, 3rd ed.; John Wiley & Sons: New York, 2002; p xviii.
(32) Fang, M.; Baldelli, S. *J. Phys. Chem. Lett.* **2015**, *6*, 1454−1460.
(33) Cimatu, K.; Baldelli, S. *J. Phys. Chem. C* **2007**, *111*, 7137−7143.
(34) Han, Y.; Raghunathan, V.; Feng, R. R.; Maekawa, H.; Chung, C. Y.; Feng, Y.; Potma, E. O.; Ge, N. H. *J. Phys. Chem. B* **2013**, *117*, 6149−6156.
(35) Lewis, I. R.; Edwards, H. G. M. *Handbook of Raman Spectroscopy: From the Research Laboratory to the Process Line*; Marcel Dekker: New York, 2001; p xiii.
(36) Cimatu, K.; Moore, H. J.; Barriet, D.; Chinwangso, P.; Lee, T. R.; Baldelli, S. *J. Phys. Chem. C* **2008**, *112*, 14529−14537.

DOI: 10.1021/acs.analchem.8b01840
Anal. Chem. 2019, 91, 1269−1276